Original Research

Corresponding author:

U. F. Dal Conte

umberto.dal.conte@external.toyota-europe.com;

+32 (0) 27124579;

Toyota Motor Europe, Hoge Wei 33, 1930, Zaventem, Belgium

Ultrasonic plastic welding of CF/PA6 composites to aluminium: process and mechanical performance of welded joints

U. F. Dal Conte [1], I. F. Villegas [1], J. Tachon [2]

[1] Faculty of Aerospace Engineering, Delft University of Technology, Kluyverweg 1, 2629HS, Delft, The Netherlands

[2] Department of Material Engineering R&D, Toyota Motor Europe, Hoge Wei 33, 1930, Zaventem, Belgium

Abstract

Due to environmental challenges and need for action with regard to CO2 emission, reducing the weight of vehicles has become one of the most important goals of car manufacturers in Europe. Materials like fibre-reinforced plastics and aluminium are the core of the research for lightweight design. However, efficiently joining these materials together is still a challenge. When thermoplastic composites are used, direct joining (i.e. without adhesives or fasteners) with the metal substrate can be obtained using welding technologies which melt the thermoplastic at the interface. In this study, ultrasonic plastic welding was investigated as a candidate technology for joining aluminium and carbon fibre-reinforced thermoplastics. The goal was to understand the main mechanisms involved in the welding process and how they affect the performance of the joint. Initially, the technique proved to be successful, but moderate strengths were obtained. Therefore, several surface pre-treatments of the aluminium were analysed to improve performance in terms of lap shear strength; mechanical, chemical and physical treatments were carried out. With laser structuring, strengths comparable to adhesive bonded joints were obtained, but in a much shorter process time. Other treatments led to considerable improvements as well. The encouraging results achieved represent an important step in the development of ultrasonic plastic welding for multi-material joining in the automotive industry.

Keywords

Ultrasonic welding; thermoplastic; composites; multi-material joining; aluminium

Introduction

In the automotive industry, the development and use of lightweight materials are crucial to reduce CO2 emissions. EU legislation set mandatory emission reduction targets for car manufacturers, which goal is to obtain a fleet average of 95 grams of CO2 per kilometre by 2021. As a result, materials like aluminium and fibre-reinforced plastics (FRPs) are finding new applications thanks to their high strength-to-weight ratio.

To fully take advantage of the specific properties of each material, effective multi-material joining technologies need to be established. Current common joining methods are mainly based on mechanical fastening and adhesive bonding, which have been applied in the industry for several decades. However, they both present several drawbacks, such as added weight and stress concentrations or chemical related issues and long processing times.

A third well-known technique generally applicable to joining of fibre reinforced thermoplastics is welding, also known as fusion bonding. Even though there are many different welding technologies involving direct metal/polymer bonding (i.e. without adhesive or fasteners), all share similar working principles: the polymer at the interface is brought to a viscous state by applying heat and subsequently the two surfaces are brought into intimate contact, followed by cooling under pressure for consolidation [1,2]. Direct adhesion between the metal surface and the thermoplastic matrix occurs in this type of joints. Mechanical interlocking and adsorption are therefore believed to have the biggest influence on joint strength [3,4]. Mechanical interlocking originates from the molten polymer which spreads into the metal surface asperities. Adsorption is based on physical interaction between the polymer and the metal, where hydrogen and Van der Waals bonds are formed at the interface. Thermoplastics are usually chemically inert, so chemical bonding with metals is not expected.

Among all different welding technologies, ultrasonic plastic welding (USPW) was chosen for this research because of its very promising features: extremely fast process times, high strengths for thermoplastic-to-thermoplastic welding, good reproducibility, low energy input and the possibility of automation [5]. The technique uses ultrasonic vibration perpendicular to the welding surface to introduce frictional heat at the interface and allows bonding to occur. The ultrasonic welding process mainly consists of a vibration phase followed by a solidification phase. The main process parameters are the amplitude and duration of the vibration and the welding force, but also material parameters like topography, geometry and physical properties affect the final result. As an indirect approach to define the duration of the vibration phase, sonotrode displacement has been successfully used as a control parameter [3,6]. A common practice in USPW of thermoplastic polymers and composites is the use of so-called energy directors (EDs). These can be either some shaped protuberance or flat films at the interface between the two joining partners (Figure 1). They consist only of neat polymeric material which experiences larger strain than the bulk material because of the lower stiffness [7] leading to preferential melting at the interface. To optimize the process and obtain good consistent weld quality, power and displacement curves can be used to establish a correlation

between the feedback of the ultrasonic plastic welder and the physical changes at the welding interface [6].

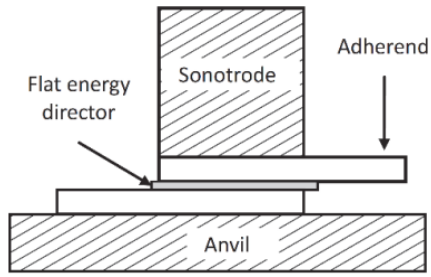

Figure 1: Schematic of the USPW process with flat energy director [7]

The literature on other metal-thermoplastic welding methods was examined as well to gain insight on the factors affecting adhesion. Ultrasonic metal welding [5,8–14], resistance welding [15,16], induction welding [17–19], friction spot joining [4,20] and laser welding [21–26] were found in literature as potential options for metal-thermoplastic welded joints. In all cases, adhesion was mostly based on mechanical interlocking and on adsorption (i.e. physical forces between the substrates). Most of the literature indicated the need for surface treatment of the metal substrate for significant improvement of the joint strength. These surface treatments ranged from mechanical treatments such as sandblasting to complex electrochemical processes like anodizing.

The goal of this experimental study was to investigate ultrasonic plastic welding as a candidate technology for direct joining of aluminium (Al) to carbon fibre-reinforced thermoplastics (CFRTPs). Initially, differences and similarities with thermoplastic-to-thermoplastic welding were assessed to understand how the existing knowledge of the welding process can be applied to metal-to-thermoplastic welding. Then, the ability of several surface treatments on the aluminium substrates to improve the lap shear strength of the welded joints was investigated.

Experimental

Materials and manufacturing

Aluminium and CFRTP substrates were used to produce the dissimilar-material welds investigated in this study. The aluminium plates were manufactured by Constellium (6061 Al alloy with TiZr coating) and the CFRTP plates were obtained from Bond-Laminates (Tepex Dynalite 202-C200, 2/2 twill woven $[0/90]_9$). The substrates to be welded were water-jet cut to their final dimensions (25mm x 100mm) from the larger Al and CFRTP plates. Table 1 summarizes the main characteristics and properties of these substrates. The geometry studied was a single-lap joint, with an overlap of 12.7mm x 25mm conforming to the ASTM D1002 standard. For the energy directors, neat PA6 film (Akulon F136-E1 by DSM Engineering Plastics) was chosen. As general procedure, two 0.12mm-thick PA6 films were stacked and consolidated by hot pressing (2MPa at 210°C for 10 minutes, heating and cooling rates of 7°C/min) obtaining an ED film with a

final thickness of 0.24mm. This value was chosen based on typical ED thicknesses used in thermoplastic-to-thermoplastic welding [6-7]. After the consolidation of the ED film, individual EDs of about 30mm x 30mm dimensions, i.e. large enough to cover the whole overlap area, were cut.

Table 1: Properties and characteristics of the materials employed in the research

Ref.	Material Characteristics	Thickness [mm]	*E* [GPa]	*σ* [MPa]
Al	6016, TiZr coating	0.9	72[1]	244[1]
CFRTP	CF/PA6, 3k 2/2 twill woven, $[0/90]_9$, 50% V_f	2	48[2]	770[2]
ED	PA6 film	0.24	/	/

[1] Tensile modulus and strength (JIS Z 2241)

[2] Flexural modulus and strength (ISO 14125, dry). *Tepex datasheet*

PA6 is well known for being hygroscopic. Consequently, to avoid unwanted moisture in the materials, all EDs and CFRTP substrates were vacuum-dried at 110°C for at least 16h in a Heraeus Vacutherm oven and subsequently allowed to cool down to room temperature (RT) out of the oven before welding. Substrates and welded joints were then kept in a desiccator prior to further testing or analysis.

To properly assess the performance of the welded joints, adhesive bonding was chosen as the reference joining technology. The adhesive used was paste epoxy Betamate 1822, supplied by Dow Automotive. Both metal and CFRTP samples were only degreased with solvent HYSO QD by Socomore before bonding and glass beads with diameters between 200µm and 300µm were used to control the bondline thickness. The adhesive was applied over an area of 12.7mm x 25mm, leaving spew fillets at the edges of the overlap. Small clamps were used to apply pressure during curing of the adhesive and to obtain the required bondline thickness. The joints were then put in a Votsch VTU oven at 180°C for 30 minutes to allow the adhesive to cure, following the supplier's instructions.

Surface treatments

Initially, the metal substrates were only degreased with solvent HYSO QD. Subsequently, different types of mechanical, chemical and physical surface treatments were used on the metal substrates to investigate their influence on the mechanical properties of the joint. Mechanical surface treatments included sandblasting, laser structuring, 3D printing of metal pins and micro-forming of metal hooks. The main goal of the mechanical treatments was to increase roughness and bonding area to enhance mechanical interlocking. As chemical surface treatments, etching and conversion coating were tested. These were used to remove weak oxide layers on the Al substrates, to

promote adsorption and, tentatively, the formation of chemical bonds with the thermoplastic polymer. Finally, plasma was used as physical surface treatment with the aim to remove contaminants from the metal surface and to promote adsorption.

Sandblasting

Sandblasting was performed manually in a sandblasting cabinet, using alumina particles with diameters between 0.35mm and 0.5mm. The alumina particles were shot perpendicular to the surface of the Al substrates from a distance of approximately 10cm for about 10 seconds.

Laser structuring

In collaboration with Fraunhofer Institute for Laser Technology (ILT, Germany), laser beams were used to machine micro-grooves on the surface of the aluminium substrates [26]. Two different types of laser structuring were performed as described in Table 2.

Table 2: Main characteristics laser structuring

Mode	Speed	Passes	Pitch distance	Groove depth	Power
Galvo Scanner	15 m/s	2	≈200µm	≈75µm	1kW
Polygon	25 m/s	7	≈300µm	≈400µm	2kW

With the Galvo Scanner mode (Table 2) the grooves presented a rounded V-shaped notch geometry (Figure 2-A). With the Polygon mode (Table 2), the grooves were deeper and featured a drop shape (Figure 2-B) aimed at increasing mechanical interlocking.

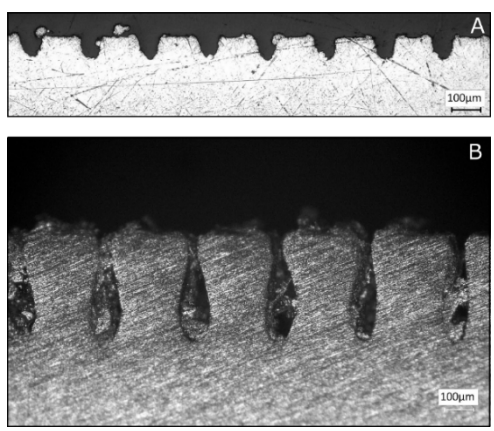

Figure 2: Grooves produced by laser in Galvo Scanner mode [A] and in Polygon mode [B]

3D printing

With the help of JP3D-TecVision (Straubing, Germany) pins were 3D-printed on the aluminium substrates. The 3D printing technology was based on selective laser melting (SLM) which uses high-power density laser to melt and join metallic powders together [27]. Eighteen conical pins with a cylindrical base (⌀=2mm, *h*=1mm) were printed on each substrate (Figure 3).

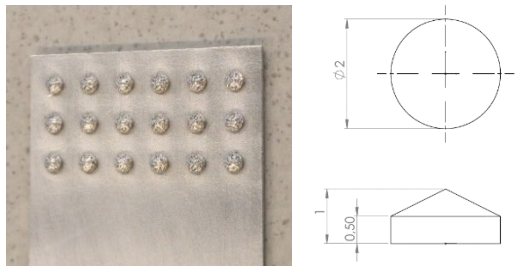

Figure 3: 3D printed pins on aluminium specimen (dimensions in mm)

Metal Hooks

The Grip-Metal™ micro-forming technology developed by Nucap Industries (Canada) was used to create an array of 1mm-high hooks with a straight profile (Figure 4).

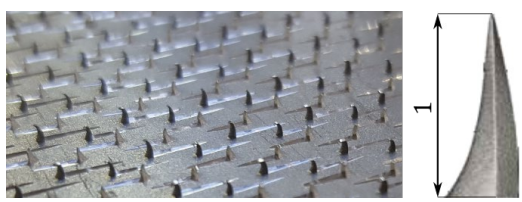

Figure 4: Hooks created on the aluminium surface (dimensions in mm)

Etching

Among the chemical surface treatments, etching of aluminium is one of the most common treatments in industry. It results in removal of the existing oxide layer and the creation of a new, more stable oxide layer.

Alkaline-acid etching is frequently used for aluminium treatment prior to adhesive bonding [28,29] and was as well used for induction welding of Al-CFRTP joints [19]. Therefore, alkaline-acid etching was used is this work. As the first step in the alkaline-acid etching procedure, the substrates were immersed in an alkaline NaOH solution for 15 minutes to dissolve any oxide on their surfaces. Subsequently, they were rinsed in distilled (DI) water and immersed in an acid solution with HNO_3 for 5 minutes to remove any oxide deposit. Finally, they were again rinsed in DI water and dried with compressed air.

A second etching, in particular acid pickling, procedure, based on the work of Bolt [3] and Mitschang et al. [19], was used as well. Following this procedure, the substrates were immersed in HNO_3 at 65% concentration for 15 minutes and then rinsed in DI water and dried with compressed air.

Conversion Coating

Conversion coatings are good alternatives to more complex chemical surface treatments, such as anodizing, to improve the durability of adhesive bonds [30,31]. A BONDERITE conversion coating solution (M-NT 30002) by Henkel was used in this work. This solution is based on Cr^{3+} and Zr which form a zirconium and chromium oxide. The substrates were cleaned in an alkaline NaOH solution for about 30 seconds and then dipped during 60s in a solution with 3 vol% of the conversion coating solution (pH between 4 and 4.3), following the supplier's instructions. Subsequently, the substrates were rinsed in DI water and dried with compressed air.

Plasma

Air plasma surface treatment was used as generated by a plasma system Tigres CKG-20 with a corona discharge gun. The aluminium substrates were placed on a support to bring the surface to be treated in contact with the plasma cloud. The support was moving at 5mm/s under the corona discharge gun, with double passage per sample.

Welding process

Welding was performed using a Rinco Dynamic 3000 ultrasonic plastic welder, which provides mechanical vibrations at 20kHz frequency and 3000W maximum power. A cylindrical titanium sonotrode (⌀=40mm) was used in this study. For specimen clamping, a steel jig designed to obtain a constant welding area of 12.7mm x 25mm and to prevent shifting of the two substrates was used (Figure 5). Thanks to a sliding platform, the welding jig also allows for vertical movement of the top substrate to minimize bending during squeeze flow of the energy director.

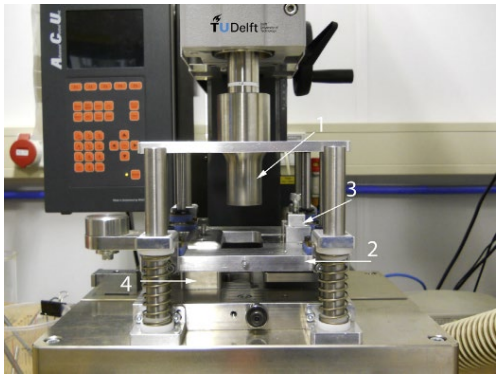

Figure 5: Ultrasonic plastic welder and clamping jig: 1) sonotrode 2) sliding platform 3) upper clamp for top substrate 4) lower clamp for bottom substrate [6]

Generally the welding force was set to 500N (≈1.5 MPa pressure on the overlap area) and the vibration semi-amplitude was set to 34.5µm. The vibration phase ended once the sonotrode reached a defined downward displacement.. This was set to 0.24 mm, i.e. same as the initial thickness of the ED, which was found to provide welds with sufficient quality. For a certain material combination, the duration of the vibration phase mainly depends on the welding force and amplitude. Values of ≈1 second were typically obtained with the selected substrates. After the vibration phase, a 500N consolidation force was applied for 4 seconds. During welding, power, displacement, energy and time were recorded and the power-displacement curves were used to interpret the physical changes occurring at the interface. Welding with the aluminium substrate as top substrate and, alternatively, as bottom substrate were investigated. In the first case, a 0.05mm-thick polyimide (Kapton) film was placed between the top Al substrate and the sonotrode to prevent fretting damage on the surface of the former.

Testing and analysis techniques

Surface characterisation

The welding surfaces of the Al substrates were characterised through the analysis of their morphology, chemical composition, topography and wettability. The surface morphology was qualitatively analysed using scanning electron microscopy (SEM) on a JEOL JSM-7500F Field Emission Scanning Electron Microscope. Using the same SEM equipment, the chemical composition of the surface was quantitatively assessed through energy-dispersive X-ray spectroscopy (EDS) analysis. To obtain a quantitative evaluation of the surface roughness provided by the different surface treatments on the Al substrates, a confocal microscope (Olympus Lex OLS3000) was used. This confocal microscope allows quantifying, the arithmetical mean height of the surface (R_a) and the root mean square height of the surface (R_q) in a 256x192 μm^2 area. Finally, the general adhesive properties of the surface were assessed through contact angle, i.e. wettability, measurements. Contact angle measurements were done on at least four different samples per treatment using a 5ml droplet of distilled water and a Theta Optical Tensiometer by Attension.

Mechanical testing

Single lap shear tests were performed on the welded samples according to the ASTM D1002 standard using a Zwick 10kN tensile testing bench. Tabs were used to align the weld line with the applied load. A grip-to-grip separation of 130mm and a testing speed of 1.3mm/minute until joint failure were set in the test. A preload of 10N was also set to guarantee tensile stresses in the joint at the beginning of the test. Lap shear strength (LSS) was obtained considering the nominal welding area. At least three welded samples were mechanically tested for each one of the different configurations considered in this study. To check the statistical relevance of the results, a single factor ANOVA analysis with a significance level of 0.05 was carried out.

Microscopy

To perform cross-section microscopic analysis of the welded joints, samples were cut from welded overlaps (see Figure 6) they were embedded in epoxy resin, ground and polished with a Struers automated polisher. A KEYENCE VHX-2000 optical microscope was used for this purpose. For fractographic analysis, SEM (JEOL JSM-7500F) was used. The thermoplastic composite substrates and samples embedded in epoxy were gold sputtered by a rotary-pumped modular coating system EMS150R by EMS before SEM observation to avoid electrical charging.

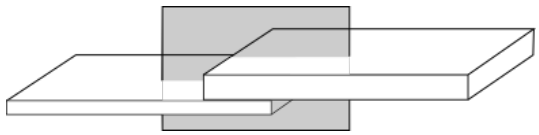

Figure 6: Schematic of a welded sample and of the cutting plane for cross-sectional microscopy samples.

Temperature measurements

Measuring the temperature at the interface in ultrasonic plastic welding is challenging since the overlap area is not easily accessible for infrared measuring, while thermocouples between the substrates are protuberances that might themselves act as energy directors and alter the process.

To overcome this problem, 0.1mm-diameter K-type thermocouples were embedded into some of the EDs (one thermocouple per ED as shown in Figure 7). The intent was to have the thermocouple tip in the center of the overlap. To manufacture these "instrumented EDs", four 0.09mm-thick PA6 films were stacked with the thermocouple sandwiched in their middle plane and the pressing procedure outlined in Section 2.1 was followed. It should be noted that the thickness of the instrumented EDs, 0.36mm, was 50% higher than that of the original EDs, 0.24mm. This increase in thickness was aimed at obtaining a flat ED surface, despite the embedded thermocouple, and hence to minimising alterations of the welding process caused by the presence of the thermocouple. Nevertheless, it should be taken into account that a higher thickness of the ED can be expected to affect heat generation at the interface. According to Palardy et al. [32], thicker EDs cause overall slower heating of the substrates since dynamic strains decrease in both the substrates and the ED when the thickness of the latter increases. Such impact on the heat generation at the entire welding overlap was however deemed more acceptable for the purpose of this research than local heat generation gradients caused by protruding thermocouples.

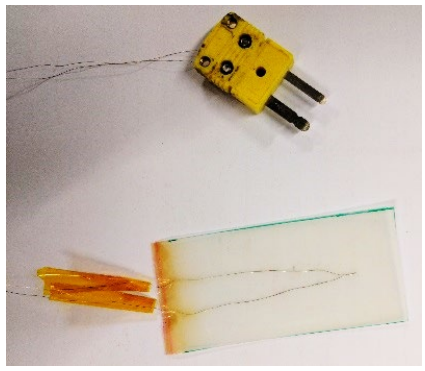

Figure 7: Thermocouple embedded in the energy director

The thermocouple output was acquired and recorded using a 10 Hz TC-08 Thermocouple Data Logger by Pico Technology. The authors are aware of the fact that a faster acquisition system would be more adequate for the intended application (note that the acquisition rate amounted to only ½ of the frequency of vibration of the ultrasonic welding process) however such a system was not available at the time this research was performed. Such limitation in the data acquisition speed was nevertheless accounted for in the interpretation of the temperature readings. The reader should also note that a set of temperature measurements was considered valid only if the tip of the thermocouple was found to be located in the centre of the overlap after fracturing of the welded joint.

Results and discussion

Welding process

The power and displacement curves provided by the ultrasonic welder for the Al to CFRTP welds showed similar features as those obtained in purely CFRTP welding processes and reported in literature [6]. In essence, the power curve featured two main peaks and the displacement curve featured a steep increase at roughly the onset of the second power peak (Figure 8-A). From the research on CFRTP welding it is known that the first peak in the power curve is related to the occurrence of melting in the energy director, whilst the second peak is linked to the occurrence of melting at the surface of the substrates. Therefore, optimum welding conditions are found around the second power peak. Beyond the second power peak bulk heating, accompanied by fibre distortion, porosity and drop in mechanical properties occurs [6,7]. Similarly to CFRTP welding, successful Al to CFRTP welds were also created around the second power peak. However, the defects or loss of strength usually attributed to welds performed beyond that peak were not observed in the Al to CFRTP welds. This was at least the case when they were welded up to a sonotrode displacement (i.e. the parameter used to indirectly control the duration of the vibration during the welding process) equal to the initial thickness of the energy director, as done in this study. The vibration time needed to reach such displacement target was found to lie between 1000 and 1100ms.

The power and displacement curves in Figure 8-A correspond to samples in a configuration in which the aluminium substrate was on top of the welding stack, i.e., in

contact with the sonotrode during the welding process (Al/CFRTP configuration). In the opposite case, i.e. when the aluminium substrate was at the bottom of the welding stack and hence in contact with the welding jig (CFRTP/Al configuration), power and displacement curves such as the ones shown in Figure 8-B and Figure 8-C were obtained. Note that when referring to a welding stack configuration by material_1/material_2, the first term refers to the material of the top substrate and the second term refers that of the bottom substrate. The main observation that can be made when comparing Figure 8-A and Figure 8-B is that the time until the occurrence of the second power peak, and hence the onset of melting on the surface of the CFRTP substrate, was significantly delayed for the CFRTP/Al configuration. In fact, the vibration time needed to reach the target 0.24mm sonotrode displacement was in this case around 1600ms, i.e. around 500ms longer than in the Al/CFRTP case. Likewise, the samples welded in the CFRTP/Al configuration could be easily detached by hand after the welding process (unsuccessful welded joints), which was not the case for the samples welded in the Al/CFRTP configuration (successful welded joints). In the previous studies by Villegas et. al [6-7], only the occurrence of the second peak was linked to the quality of the weld. The height and width of the peaks are possibly linked to the properties of the adherends themselves, but this has not been investigated thoroughly yet.

Since the welding stack had the same composition in both the Al/CFRTP and the CFRTP/Al configurations it can be assumed that heat was generated at the same rate in both cases. Consequently, slower heating of the CFRTP substrate in the CFRTP/Al configuration should be attributed to faster heat dissipation from the welding interface into and through the Al substrate. In the CFRTP/Al configuration the Al substrate rested completely on the base of the steel welding jig whereas in the Al/CFRTP configuration only the overlap area in the Al substrate was in contact with the titanium sonotrode. The difference in contact area as well as in thermal conductivity between steel and titanium could account for bigger heat dissipation through the Al substrate into the steel jig and consequently slower temperature build-up at the welding interface in the CFRTP/Al configuration.

Temperature measurements at the welding interface in both the Al/CFRTP and the CFRTP/Al configurations confirmed the hypothesis above. Despite the limitations of the temperature measuring setup, as explained in Section 2.3, the results consistently showed significant differences in the maximum temperature measured at the welding interface in the Al/CFRTP configuration, around 490°C, and the CFRTP/Al configuration, around 350°C. Furthermore welding experiments were performed on the CFRTP/Al configuration in which a 125µm-thick Kapton film was placed between the Al substrate and the welding jig. Successful welded joints were obtained and the corresponding power and displacement curves showed indeed a shortening in the time needed to reach the second power peak and in the time needed to reach the target sonotrode displacement (around 1200ms) as seen in Figure 8-C. Besides, when comparing LSS between welds from Figure 8-A and Figure 8-C (successful welded joints), a slightly higher LSS was obtained (+8.3%) when Al was the bottom substrate and the Kapton film was used. This could be linked to the thermal insulating effect of the Kapton film, which resulted in increased adhesion between the substrates. Based on these results and to prevent damage of the sonotrode (designed for plastic welding) all the

subsequent welds performed in this research were obtained in a CFRTP/Al configuration with a 125µm-thick Kapton film between the Al substrate and the welding jig.

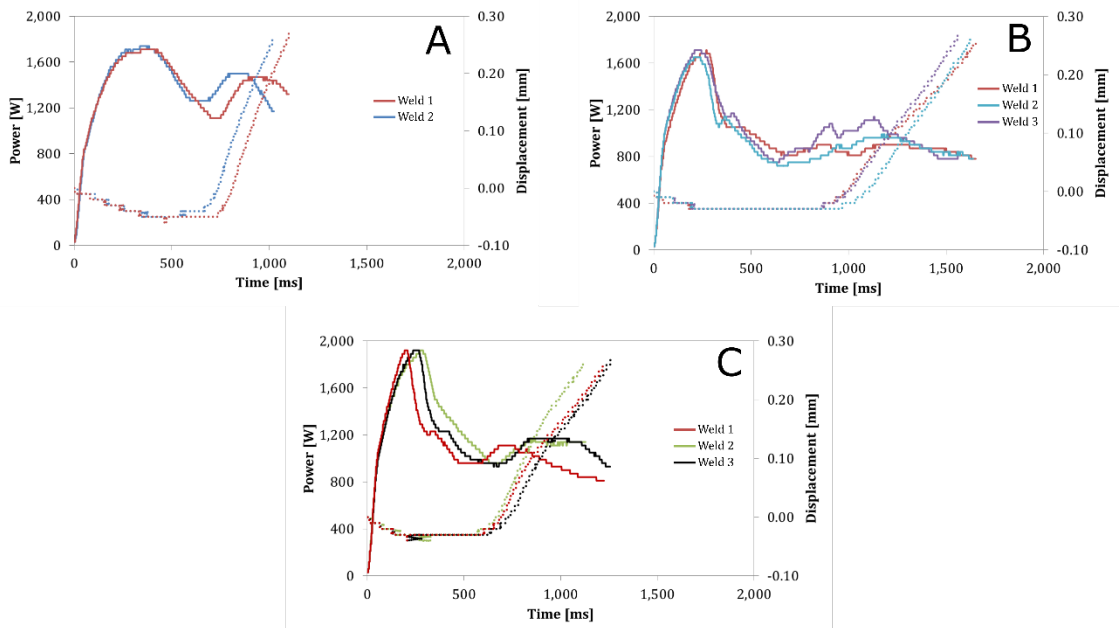

Figure 8: Power and displacement curves for the (untreated) Al/CFRTP configuration (Al as top substrate) [A]; for the CFRTP/(untreated) Al configuration (Al as bottom substrate) [B]; for the CFRTP/(untreated) Al configuration (Al as bottom substrate) with a 0.10mm-thick Kapton film between the Al substrate and the jig [C]

Surface treatments

Surface morphology

The surface of a substrate not subjected to any pre-treatments other than degreasing can be seen in Figure 9-UT. This Figure shows a lightly textured surface with impurities. Sandblasting produced a much rougher surface (Figure 9-SB) with irregular morphology and practical absence of impurities. The grooves created by the laser treatment are shown in Figure 9-LAS (GS) for the Galvo Scanner mode and in Figure 9-LAS (POL) for Polygon mode (Table 2). In these figures it is possible to see the differences in pitch distance, groove width and groove depth between the two types of laser treatment. It is also possible to see residues of the laser structuring process on the surfaces as well as significant deformation of the material at the edges of the grooves.

Plasma treatment (Figure 9-P), and acid pickling (Figure 9-AP) showed clean surfaces with the same texture as the untreated samples (Figure 9-UT). The original texture was as well maintained in the substrates subjected to alkaline-etching and the conversion-coating treatment. However, the alkaline-etching treatment produced a large amount of very small pits on the surface, most likely due to the aggressive action of NaOH (Figure 9-AA). Finally, the conversion-coating treatment formed small particles

on the surface (Figure 9-CC). These particles did however not densely cover the surface, probably due to the short immersion time of the substrates in the BONDERITE solution. The influence of parameters such as duration of treatment, concentration of the solution, temperature, etc., on the formation of the conversion layer was out of the scope of the present work but may be an interesting topic for further research.

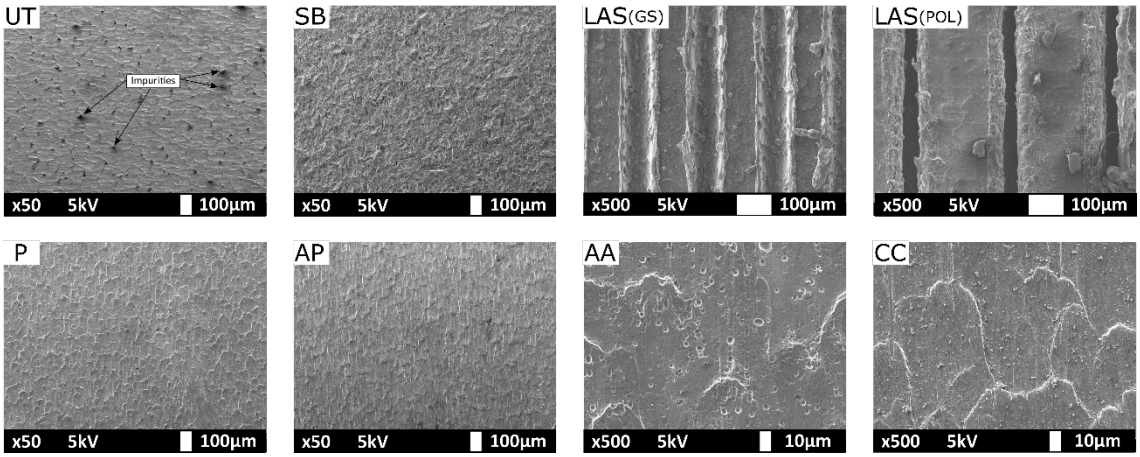

Figure 9: SEM micrographs of: aluminium surface without pre-treatments [UT]; aluminium surface after sandblasting treatment [SB]; aluminium surface with grooves created by laser in Galvo Scanner mode [LAS(GS)]; aluminium surface with grooves created by laser in Polygon mode [LAS(POL)]; aluminium surface subjected to plasma treatment [P]; aluminium surface subjected to acid pickling [AP]; aluminium surface after alkaline-acid etching [AA]; particles of the conversion coating layer on the aluminium surface [CC].

Chemical composition

Table 3 shows the composition of the aluminium surface after different treatments as obtained by EDS analysis. Alkaline-acid and acid pickling etching as well as the plasma treatment removed a large number of organic contaminants, indicated by the decreasing amount of carbon on the surface. After plasma treatment, even small amounts of titanium and zirconium were detected, probably from the original TiZr coating on the aluminium (Table 1). The presence of the chromium and zirconium conversion coating was confirmed as well. The Cr and Zr values were however small which correlates with the small amount of particles observed on the surfaces (Figure 9-CC). Alkaline-acid etching shows a higher amount of aluminium than the untreated material, which confirms the removal of the outer layer from the original surface. Conversely, a lower concentration of aluminium was found in the sandblasted substrate along with a higher amount of oxygen than on the untreated material. The results for the sandblasted material are consistent with the usage of Al_2O_3 as the blasting medium, which increased the amount of oxide on the surface. Sandblasting also increased the actual surface area, which could potentially adsorb more contaminants, hence the slightly higher amount of carbon found on it as compared to the untreated material.

Table 3: EDS chemical composition (wt%) of the aluminium surface after different treatments (UT: untreated, SB: sandblasting, AA: alkaline-acid etching, AP: acid pickling etching, CC: conversion coating, P: plasma). Measurement was done on one sample per treatment.

	UT	SB	AA	AP	CC	P
Al	75.48	65.56	82.31	76.41	70.26	76.75
O	3.12	9.66	2.08	7.78	6.54	4.66
C	20.93	23.22	14.57	14.97	21.52	16.86
Mg	0.19	0.22	0.25	0.30	0.24	0.24
Si		0.62	0.79	0.55	0.72	0.60
Ti						0.26
Zr					0.53	0.12
Cr					0.04	
Fe		0.74				
F	0.28					0.51

Surface topography

Table 4 shows the results of the roughness measurements (R_a and R_q values) on the surface of the Al substrates. As seen in this table, the chemical and physical treatments only caused a slight roughness increase. Conversely, sandblasting created a much more rough surface, as also observed in the SEM micrographs (Figure 9-SB), and hence with a larger bonding area and with the potential to effectively increase mechanical interlocking with the molten TP.

Table 4: Surface roughness values and Water contact angle measurement for aluminium surface after the different treatments (UT: untreated, SB: sandblasting, AA: alkaline-acid etching, AP: acid pickling etching, CC: conversion coating, P: plasma). Roughness measurements were done on one sample and four samples were used for water contact angle.

	UT	SB	AA	AP	CC	P
Ra	0.83	5.20	1.06	1.01	0.85	1.07

Rq	1.05	6.56	1.33	1.29	1.15	1.44
θ°	85 (±5)	72 (±6)	103 (±3)	65 (±3)	33 (±8)	34 (±4)

Surface wettability

The results of the contact angle measurements can be seen in Table 4. An example of the difference in contact angle for two different types of surfaces is shown in Figure 10.

Plasma and conversion coating showed the lowest contact angles, approximately 60% lower than untreated aluminium, revealing a better wettability and hence higher surface energy and the potential for better adhesion [33,34]. In the case of the plasma treatment the low contact angle likely resulted from the removal of contaminants from the surface (section 3.2.2). In the case of the conversion coating treatment, the low contact angle was attributed to the chemical modification of the surface as well (section 3.2.2). Acid pickling was also found to decrease the contact angle as compared to the untreated metal surface but not as much as the plasma and conversion coating treatments. A similar decrease in contact angle as that obtained with acid pickling was found on the sandblasted surfaces. Sandblasting increases the roughness of the surface and higher roughness is known to enhance wettability [35,36]. Finally and contrarily to our expectations from the EDS results, alkaline-acid etching was found to increase the wetting angle. This might have been caused by improper cleaning of the surfaces etching resulting on the presence of some residual chemicals.

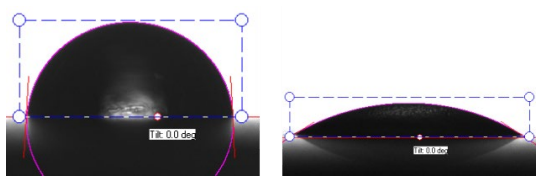

Figure 10: Example of water droplet on a non-treated sample (left) and a sample treated with conversion coating (right)

Strength and failure of welded joints

Lap shear strength

Lap shear strength results in standard conditions for welded joints with the different surface treatments used in this study are shown in Figure 11. LSS of adhesively bonded joints is included in this Figure to show how ultrasonic plastic welding compares with other joining technologies. It should be noted however that the adhesively bonded joints featured spew fillets and thicker bondlines than the welded joints (200-300 μm bondline thickness versus approximately 100 μm weldline thickness as observed in cross sectional micrographs). As a result, the stresses experienced by the adhesively bonded

and the welded joints for the same load level could be expected to differ [37–40] and hence direct comparison of LSS values should be regarded with care. In general the welded joints were produced under the conditions specified in Section 2.3 with the Al substrate as the bottom substrate separated from the jig by a 125µm-thick Kapton film as explained in Section 3.1. Nevertheless, when the Al substrates with 3D-printed pins and metal hooks were used, the displacement of the sonotrode was set to 1 mm, equal to the height of the pins and of the hooks. No PA6 energy director was used in the case of the metal hooks. Finally, the LSS values in Figure 11 for the welded samples with laser-treated Al substrates correspond to the substrates treated with the Galvo Scanner laser mode (Table 2). The grooves provided by the Polygon laser mode were too deep and ended up severely weakening the Al substrate. This led to failure of the Al substrate when subjected to the ultrasonic vibrations during the welding process. Based on this and to avoid potential damage when welding the Galvo Scanner laser-treated samples the amplitude of the vibrations was reduced in that particular case to its minimum in the used welding setup, i.e. 26 µm.

Some of the main observations from Figure 11 are described and discussed below. Firstly, the majority of the joints produced in this study showed small dispersion in their LSS values (below 5% scatter) except for the welded joints involving metal hooks on the Al substrate and alkaline-acid etching (around 10% scatter). LSS values after each treatment were compared to the LSS of untreated samples using the ANOVA analysis. The null hypothesis was rejected for all treatments except for alkaline-acid etching and metal hooks. Therefore, the effect of these two treatments on the LSS of the welded joints cannot be considered statistically relevant. Secondly, among all the welded joints produced in this study the ones with laser-treated Al substrates provided the highest LSS values. The average LSS of the laser-treated welded samples was twice as high as that of the untreated welded samples and almost at the same level as the average LSS of the reference adhesively bonded samples. The samples welded after conversion-coating and sandblasting treatments resulted in LSS values approximately 50% higher than those of the untreated welded samples. Acid pickling and plasma treatments provided an approximately 25% LSS increase with respect to the untreated welded samples. Contrarily, 3D printed pins, metal hooks and alkaline-acid etching did not seem to result in any significant improvement of the LSS of the welded joints.
When comparing these results with LSS obtained by Balle et al. for ultrasonic metal welding of CFRTP to Al [5], lower values were observed in the present work. This could be explained mainly by a different degree of mechanical interlocking between CFRTP and metal obtained through the ultrasonic metal welding process. However, a direct comparison should be made with care since materials, testing and specimen configurations were different.

These results were roughly in accordance with the trends observed in the wettability tests for the sandblasting, conversion-coating, plasma, acid pickling and alkaline-acid etching treatments. The results obtained for mechanical treatments with through-the-thickness reinforcements, i.e. metal pins and hooks, were however surprisingly low according to our expectations. To further understand the effects of the pre-treatments on the strength of the welded joints, cross sections and fracture surfaces were analysed.

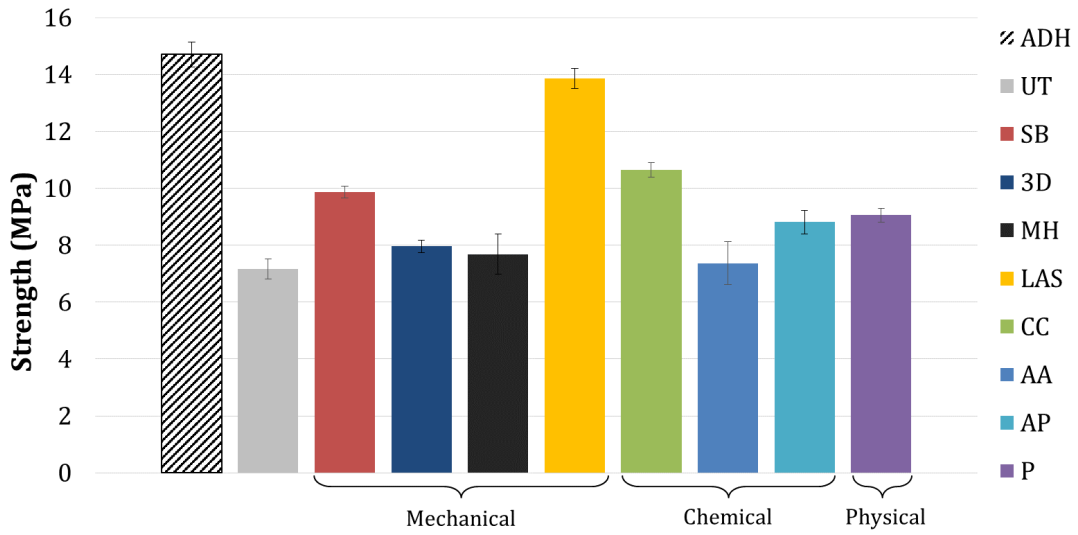

Figure 11: Lap shear strength of welded joints for different treatments on the Al substrate and of adhesively bonded joints (reference). ADH: adhesive, UT: untreated, SB: sandblasting, 3D: 3D printed pins, MH: metal hooks, LAS: laser, CC: conversion coating, AA: alkaline-acid etching, AP: acid pickling and P: plasma.

Fractographic and cross-section analysis

Fracture surfaces of all the welded samples, except for those with through-the-thickness reinforcement (3D-printed pins and metal hooks), showed similar features. In particular, a narrow band at the edge of the overlap showed presumably composite (first-ply) failure, in the form of resin and reinforcement fibres which remained adhered to the Al substrate after failure of the welded joint. The rest, i.e. majority, of the overlap displayed adhesive failure, i.e. no visible traces of resin or fibre reinforcement on the Al substrate after failure of the welded joint. These features, shown in Figure 12 for a welded sample with untreated Al substrate, were, as already mentioned, also found in samples with treated Al substrates. The main difference was that, in the case of treatments found to cause a moderate increase of the LSS, such as sandblasting, conversion coating and plasma, (see Figure 11), the area featuring composite failure was seen to increase as compared to the welded joints with untreated Al substrates (see Figure 13 vs. Figure 12). Consequently, in the welded joints the Al-CFRTP adhesion strength was found to locally surpass the interlaminar strength of the CFRTP, which could be regarded as a sign of good adhesion, but this was only achieved in a small portion of the overlap.

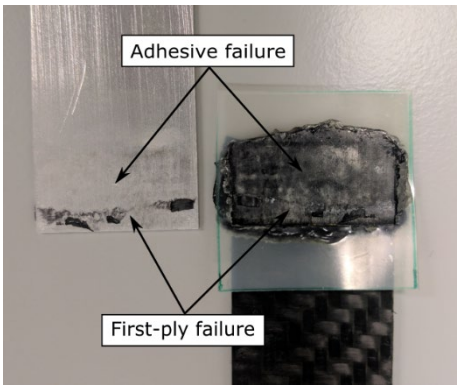

Figure 12: Fracture surfaces of CFRTP/(untreated) Al. Different types of failure are visible along the overlap

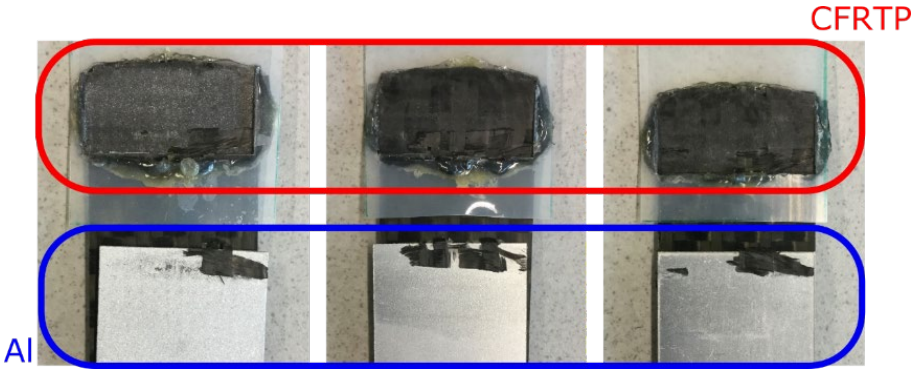

Figure 13: Fracture surfaces of joints between CFRTP and aluminium treated with sandblasting (left), conversion coating (center) and plasma (right)

The case of welded joints with laser-treated Al substrates, which resulted in the highest LSS values among all the welded joints considered in this study (Figure 11), is no exception to these failure features as shown in Figure 14. It is interesting to note that despite that fact that, as discussed before, only a small portion of the welded overlap featured good adhesion the LSS of the welded joints was very close to the LSS of the reference adhesive joints, which featured cohesive failure, and hence good adhesion, in the complete overlap. Closer inspection of the welded joints with laser-treated Al substrates revealed significant plastic deformation of the thermoplastic resin in the areas where composite failure occurred, which most likely contributed to the relatively higher single lap shear strength values observed for this configuration. Inspection of the areas featuring adhesive failure revealed clean grooves on the Al fracture surface and corresponding resin protrusions on the CFRTP fracture surface. This indicates that melting and flow of the thermoplastic resin also occurred in these areas, which resulted in an increased contact area between Al and the thermoplastic resin as compared to the reference untreated Al substrate and hence increased LSS. Finally some cracks could be observed within the grooves in the laser-treated Al substrate, caused by either the ultrasonic vibration during the welding process or the single lap shear test itself.

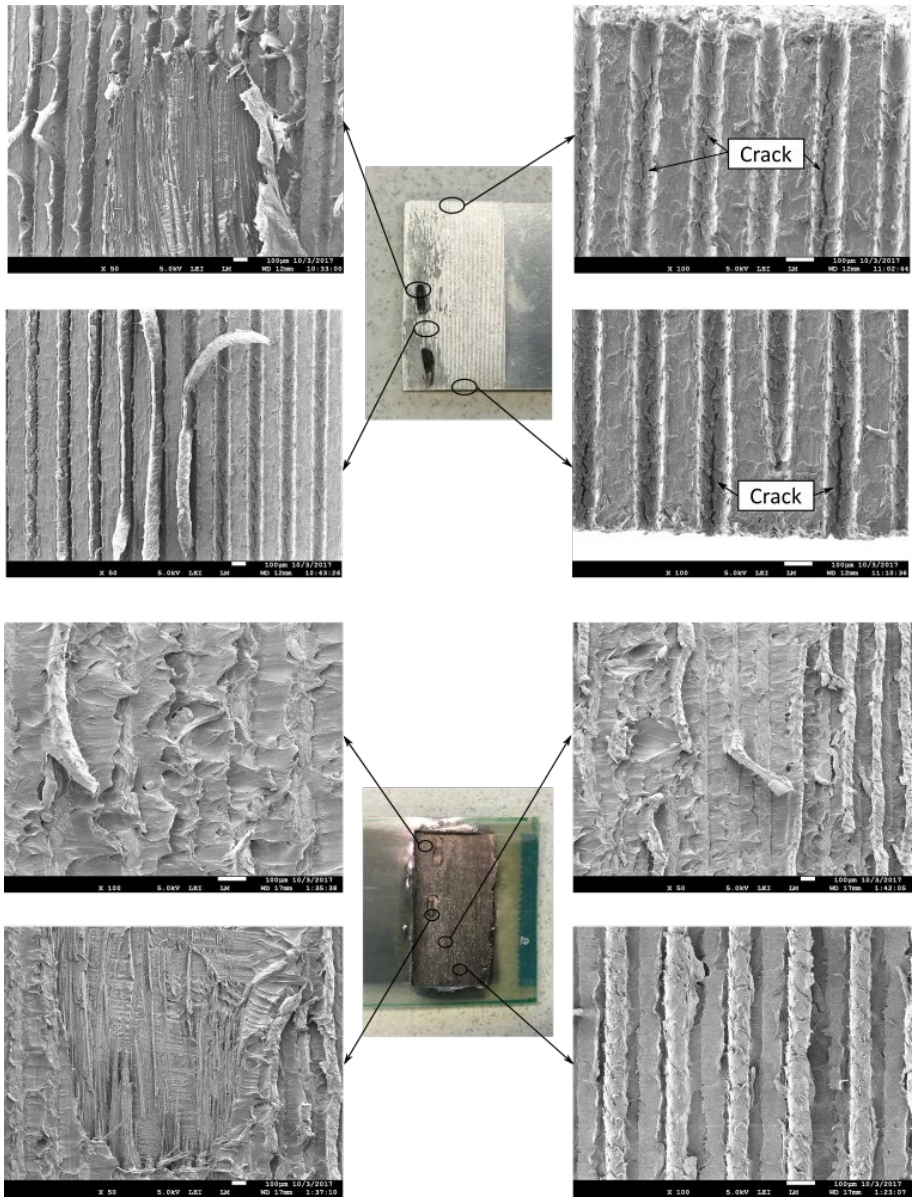

Figure 14: Fracture surface of the laser treated aluminium (top) and CFRTP (bottom) substrates, with details analysed by SEM.

A potential explanation to the observation that only a small area towards one of the edges of the welded overlap displayed composite failure lies on, on one hand, the fact that during the welding process the highest temperatures are developed at the edges of the overlap [16,41] and, on the other hand, on the higher thermal conductivity of Al as compared to CFRTP. Owing to the fact that the welded joints created in this study were composed of two different materials, Al and CFRTP, the two edges of the overlap had very distinct boundary conditions. Specifically while one of the edges, denoted as “CFRTP edge” in Figure 15, was in direct contact with the rest of the Al substrate, the other edge, denoted as “metal edge” in Figure 15, was in direct contact with the rest of the CFRTP substrate. This means that heat generated at and in the vicinity of the CFRTP edge was more easily

dissipated into the colder Al substrate than it was dissipated into the colder CFRTP substrate at the metal edge. Consequently, higher temperatures were achieved at the metal edge, leading to a lower viscosity of the molten polymer which could thus better conform to the micro-topology of the Al substrate resulting in stronger adhesion through micro-mechanical interlocking. This is supported by the results of the cross-section analysis at the metal and CFRTP edge of a welded sample shown in Figure 16, which evidence the inability of the polymer to conform to the surface asperities of the (untreated) Al substrate at the CFRTP edge as opposed to what happens at the metal edge.

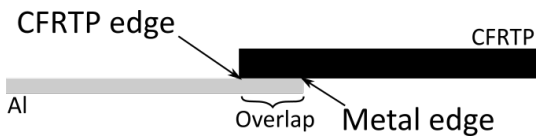

Figure 15: Schematic of welded sample with definition of metal and CFRTP edges of the overlap.

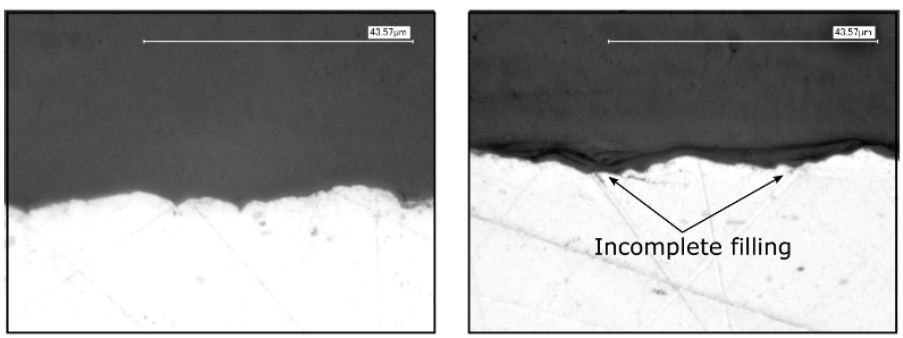

Figure 16: Cross section micrographs of CFRTP/(untreated) Al interface close to the metal edge (left) and to the CFRTP edge (right). Differences in how the polymer conforms to the asperities on the Al surface are apparent.

Regarding the samples with through-the-thickness reinforcements, Figure 17 (left) shows the fracture surfaces of a welded joint in which the Al substrate was provided with 3D-printed pins. This result indicates that during mechanical testing the metal pins were cleanly extracted from the CFRTP substrate. This can be attributed to the peel stresses present in the single lap shear test and to the lack of anchoring of the pins within the CFRTP owing to their convex morphology (see Figure 17, right). The case in which the Al substrates were provided with metal hooks is however different, since fracture surfaces showed a combination of hook pull-out from the CFRTP substrate and from the Al substrate as well (see Figure 18, top). Hook pull-out from the CFRTP substrate can be explained by severe deformation of the hooks during the welding process resulting in a convex shape with little to no anchoring in the CFRTP substrate (see Figure 18, bottom). Hook pull-out from the Al substrate can be explained by damage caused in the hooks during the welding process resulting in cracks as shown in Figure 18, bottom. It should as well be noted that, contrarily to the other surface treatments considered in this work, the pins and hooks led to quite uniform fracture surfaces which indicates quite uniform weld quality along the overlap.

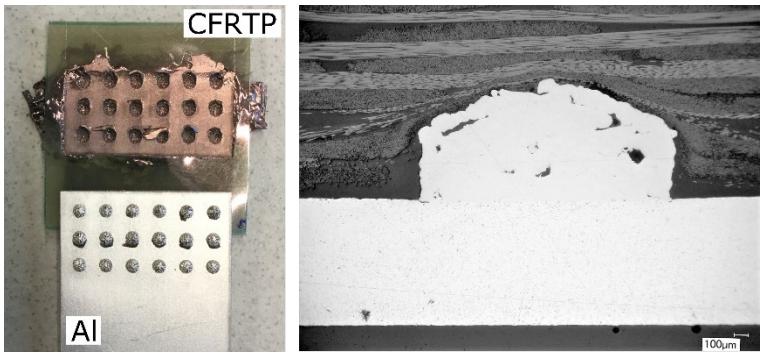

Figure 17: Fracture surfaces (left) and cross section micrograph (right) of welded joint in which the Al substrate was provided with 3D-printed pins.

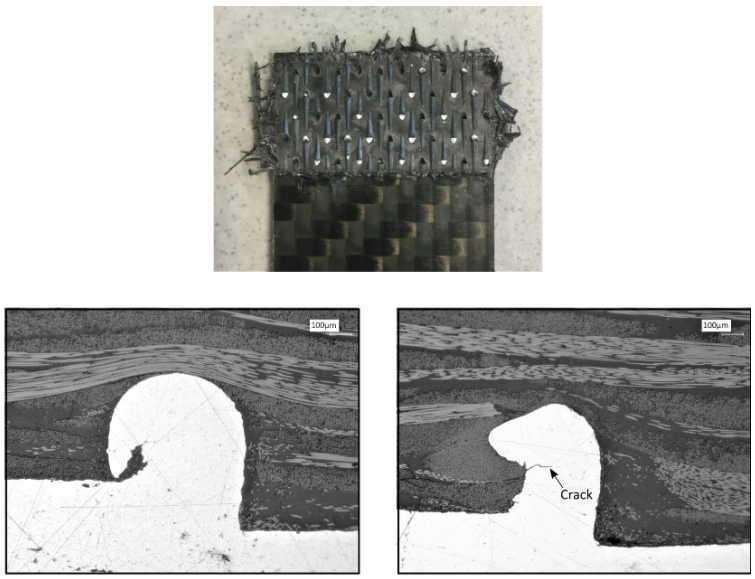

Figure 18: CFRTP fracture surface (top) and Cross section micrographs (bottom) of a welded joint in which the Al substrate was provided with metal hooks.

Conclusions

Multi-material joining is considered an important challenge in the automotive industry, with several advanced technologies still in development. In this experimental study, ultrasonic plastic welding was investigated as a candidate technology for direct joining (i.e. without adhesive or fasteners) between aluminium and CFRTP (CF/PA6). The following main conclusions were drawn from the results of this study:

Ultrasonic plastic welding of Al-CFRTP joints with flat energy directors and displacement-controlled welding process provided welded joints which, with an adequate surface treatment of the Al substrate, resulted in similar lap shear strength values as the reference adhesively bonded joints. The total time (vibration and solidification time)

required to produce each welded sample amounted to 5 seconds as opposed to the 30min curing time for the adhesively bonded joints.

The higher thermal conductivity of Al as compared to that of CFRTP was found to make ultrasonic plastic welding of CFRTP to Al more sensitive to boundary conditions than ultrasonic welding of CFRTPs. In particular, the position of the Al substrate (partially in contact with the sonotrode at the top of the welding stack or totally in contact with the welding jig at the bottom of the welding stack) was found to have an effect on the duration of the welding process and on the weld strength.

Using surface treatment to increase mechanical interlocking and/or adsorption, and hence the wettability of the Al substrates, resulted in promising results. In particular laser structuring was found to provide a 100% strength increase as compared to welded joints with untreated Al substrates. However excessive weakening of the substrates caused by deep laser-carved grooves was spotted as a potential issue. Alternatively, conversion coating and sandblasting resulted in approximately 50% strength increase with regards to welded joints with untreated Al substrates.

Despite the promising strength values, the welded joints featured non-uniform adhesion quality across the welding overlap caused by the high thermal conductivity of the Al substrate. According to this only a small area of the overlap displayed sufficient adhesion as to cause composite (first-ply) failure instead of adhesive failure. This issue should be overcome in order to take full advantage of the potential of the welding process.

Pins or hooks printed or micro-formed on the surface of the Al substrate did not show improvements on the strength of the welded joints owing to geometrical issues that resulted in either insufficient anchoring within the CFRTP or damage during welding. They did however result in more uniform weld quality along the overlap.

The results obtained in this study revealed a new potential of ultrasonic plastic welding to join metals and thermoplastics. This joining technology combined with specific metal surface pre-treatments could lead to important developments in the automotive industry, offering new and valuable solutions in the assembly lines.

Acknowledgements

The authors would like to thank the following partners for the great support provided during the research study. Fraunhofer Institute for Laser Technology (ILT), Germany; Nucap Industry, Canada; JP3D-TecVision, Germany.

Funding

This research received no specific grant from any funding agency in the public, commercial, or not-for-profit sectors.

Declaration of Conflicting Interests

The Author(s) declare(s) that there is no conflict of interest.

References

1. Pereira A, Botelho EC, Costa ML, et al. A Review of Welding Technologies for Thermoplastic Composites in Aerospace Applications. *J Aerosp Technol Manag* 2012; 4: 255–265.

2. Villegas IF, Mose L, Yousefpour A, et al. Process and performance evaluation of ultrasonic, induction and resistance welding of advanced thermoplastic composites. *J Thermoplast Compos Mater* 2013; 26: 1007–1024.

3. Bolt S. Masters Thesis: Ultrasonic Plastic Welding of Carbon Fiber Reinforced Polyamide 6 to Aluminium and Steel.

4. Goushegir SM. Friction spot joining (FSpJ) of aluminum-CFRP hybrid structures. *Weld World* 2016; 60: 1073–1093.

5. Wagner G, Balle F, Eifler D. Ultrasonic Welding of Aluminum Alloys to Fiber Reinforced Polymers. *Adv Eng Mater* 2013; 15: 792–803.

6. Villegas IF. In situ monitoring of ultrasonic welding of thermoplastic composites through power and displacement data. *J Thermoplast Compos Mater* 2015; 28: 66–85.

7. Villegas IF. Strength development versus process data in ultrasonic welding of thermoplastic composites with flat energy directors and its application to the definition of optimum processing parameters. *Compos Part A Appl Sci Manuf* 2014; 65: 27–37.

8. Krüger S, Wagner G, Eifler D. Ultrasonic Welding of Metal / Composite Joints. *Adv Eng Mater* 2004; 6: 157–159.

9. Balle F, Wagner G, Eifler D. Ultrasonic Metal Welding of Aluminium Sheets to Carbon Fibre Reinforced Thermoplastic Composites. *Adv Eng Mater* 2009; 11: 35–39.

10. Balle F, Huxhold S, Wagner G, et al. Damage Monitoring of Ultrasonically Welded Aluminum / CFRP-Joints by Electrical Resistance Measurements. *Procedia Eng* 2011; 10: 433–438.

11. Balle F, Eifler D. Statistical test planning for ultrasonic welding of dissimilar materials using the example of aluminum-carbon fiber reinforced polymers (CFRP) joints. *Materwiss Werksttech* 2012; 43: 286–292.

12. Wagner G, Balle F, Eifler D. Ultrasonic Welding of Hybrid Joints. *JOM* 2012; 64: 401–406.

13. Balle F, Emrich S, Wagner G, et al. Improvement of Ultrasonically Welded Aluminum / Carbon Fiber Reinforced Polymer-Joints by Surface Technology and High Resolution Analysis **. *Adv Eng Mater* 2013; 15: 814–820.

14. Balle F, Huxhold S, Emrich S, et al. Influence of Heat Treatments on the Mechanical Properties of Ultrasonic Welded AA 2024 / CF-PA66-Joints. *Adv Eng Mater* 2013; 15: 837–845.

15. Christophe A, Ye L. Resistance Welding of Metal / Thermoplastic Composite Joints. *J Thermoplast Compos Mater* 2006; 14: 449–475.

16. Stavrov D, Bersee HEN. Resistance welding of thermoplastic composites-an overview. *Compos Part A Appl Sci Manuf* 2005; 36: 39–54.

17. Ahmed TJ, Stavrov D, Bersee HEN, et al. Induction welding of thermoplastic composites - an overview. *Compos Part A Appl Sci Manuf* 2006; 37: 1638–1651.

18. Mitschang P, Velthuis R, Emrich S, et al. Induction Heated Joining of Aluminum and Carbon Fiber Reinforced Nylon 66. *J Thermoplast Compos Mater* 2008; 22: 17–27.

19. Mitschang P, Velthuis R, Didi M. Induction Spot Welding of Metal / CFRPC Hybrid Joints. *Adv Eng Mater* 2013; 15: 804–813.

20. Liu FC, Liao J, Nakata K. Joining of metal to plastic using friction lap welding. *Mater Des* 2014; 54: 236–244.

21. Chen YJ, Yue TM, Guo ZN. A new laser joining technology for direct-bonding of metals and plastics. *Mater Des* 2016; 110: 775–781.

22. Jung K, Kawahito Y, Takahashi M, et al. Laser direct joining of carbon fiber reinforced plastic to aluminum alloy. *J Laser Appl*; 25. Epub ahead of print 2015. DOI: 10.2351/1.4794297.

23. Katayama S, Kawahito Y. Laser direct joining of metal and plastic. *Scr Mater* 2008; 59: 1247–1250.

24. Kawahito Y, Katayama S. Characteristics of lamp joining structures for several materials. In: *Proceedings of ICALEO*. 2010, pp. 1469–1473.

25. Niwa Y, Kawahito Y, Kubota S, et al. Evolution of lamp joining to dissimilar metal welding. In: *Proceedings of ICALEO*. 2008, pp. 311–317.

26. Engelmann C, Eckstaedt J, Olowinsky A, et al. Experimental and simulative investigations of laser assisted plastic- metal-joints considering different load

directions. *Phys Procedia* 2016; 83: 1118–1129.

27. Bremen S, Meiners W, Diatlov A. Selective Laser Melting. *LTJ* 2012; 9: 33–38.

28. Adhesive Bonding. *EAA Alum Automot Man – Join* 2015; 1–42.

29. Monteiro FJ, Barbosa MA, Gabe DR, et al. Surface pretreatments of aluminium for electroplating. *Surf Coatings Technol* 1988; 35: 321–331.

30. Golru SS, Attar MM, Ramezanzadeh B. Effects of surface treatment of aluminium alloy 1050 on the adhesion and anticorrosion properties of the epoxy coating. *Appl Surf Sci* 2015; 345: 360–368.

31. Nordlien JH, Walmsley JC, Østerberg H, et al. Formation of a zirconium-titanium based conversion layer on AA 6060 aluminium. *Surf Coatings Technol* 2002; 153: 72–78.

32. Palardy G, Villegas IF. On the effect of flat energy directors thickness on heat generation during ultrasonic welding of thermoplastic composites. *Compos Interfaces* 2017; 24: 203–214.

33. Adams RD. *Adhesive bonding: science, technology and applications*. 2005.

34. Baldan A. Adhesion phenomena in bonded joints. *Int J Adhes Adhes* 2012; 38: 95–116.

35. Kubiak KJ, Wilson MCT, Mathia TG, et al. Wettability versus roughness of engineering surfaces. *Wear* 2011; 271: 523–528.

36. Wenzel RN. Resistance of solid surfaces to wetting by water. *Ind Eng Chem* 1936; 28: 988–994.

37. Banea MD. Adhesively bonded joints in composite materials : an. *Proc Inst Mech Eng Part L J Mater Des Appl* 2008; 223: 1–18.

38. Ojalvo IU, Eidinoff HL. Bond Thickness Effects upon Stresses in Single-Lap Adhesive Joints. *AIAA J* 1978; 16: 204–211.

39. Crocombe A, Adams RD. Infuence of the spew fil llet and other parameters on the stress distribution in the single lap joint. *J Adhes* 1981; 13: 141–155.

40. Tong L. Bond strength for adhesive-bonded single-lap joints. *Acta Mech* 1996; 117: 101–113.

41. Levy A, Le S, Villegas IF. Modeling of the heating phenomena in ultrasonic welding of thermoplastic composites with flat energy directors. *J Mater Process Tech* 2014; 214: 1361–1371.